

Nodule2vec: a 3D Deep Learning System for Pulmonary Nodule Retrieval Using Semantic Representation

Ilia Kravets^{1,2,*}, Tal Heletz^{1,2,*}, and Hayit Greenspan³

¹ Independent Researcher {ilia.kravets,talheletz123}@gmail.com

² Y-Data, Yandex School of Data Analysis, Tel Aviv, Israel

³ Tel Aviv University, Tel Aviv, Israel hayit@eng.tau.ac.il

Abstract. Content-based retrieval supports a radiologist decision making process by presenting the doctor the most similar cases from the database containing both historical diagnosis and further disease development history. We present a deep learning system that transforms a 3D image of a pulmonary nodule from a CT scan into a low-dimensional embedding vector. We demonstrate that such a vector representation preserves semantic information about the nodule and offers a viable approach for content-based image retrieval (CBIR). We discuss the theoretical limitations of the available datasets and overcome them by applying transfer learning of the state-of-the-art lung nodule detection model. We evaluate the system using the LIDC-IDRI dataset of thoracic CT scans. We devise a similarity score and show that it can be utilized to measure similarity 1) between annotations of the same nodule by different radiologists and 2) between the query nodule and the top four CBIR results. A comparison between doctors and algorithm scores suggests that the benefit provided by the system to the radiologist end-user is comparable to obtaining a second radiologist’s opinion.

Keywords: CBIR · Pulmonary Nodules · Deep Learning · Image Retrieval

1 Introduction

1.1 Motivation and Background

Lung cancer is a leading cause of cancer mortality in both men and women, accounting for nearly 25% of all cancer deaths[16]. The chances of treating lung cancer successfully are much higher if the treatment starts at an early stage.

Currently, Low-Dose Computed Tomography (LDCT) screening is the most effective way for pulmonary nodules detection and diagnosis, and its usage has increased dramatically over the last two decades. However, scan examination and diagnosis is a very time-consuming task that requires a lot of invaluable radiologist time.

* I. Kravets, T. Heletz – equal contribution

To assist radiologists to quickly and effectively diagnose tumors, it is important to present them with similar historical cases. Examination of similar cases can be beneficial in two aspects. First, the radiologist can have access to the labeling information that other doctors gave in similar cases and thus can deduce the status of the current case. Second, the radiologist can examine the related case development history past the similarly looking LDCT scan, as if peeking at a possible future of the current case and infer a more accurate prognosis. For example, a similar case biopsy outcome can suggest whether it is advisable to perform a biopsy in the current case.

Many contemporary works that apply machine learning techniques to medical imaging aim to replace the doctors and directly produce a diagnosis. The usual downsides of this approach are the lack of the output interpretability and uncertain robustness guarantees in the light of potential bugs, input variation, or even adversarial attacks. Moreover, they are usually lacking in the amount of diagnostic data they can provide, often limited by a handful of bits of information, like benign-vs-malignant binary classification.

The solution we describe is a content-based image retrieval (CBIR) system. Given a pulmonary nodule, our system retrieves several similar nodules from the historical database, potentially enriched with the relevant clinical records, to aid the doctor in the diagnostic process. Our main contributions include:

- We develop a system to provide the radiologist semantically-meaningful decision support in nodule analysis, in contrast to providing an automated nodule diagnosis.
- We identify architectural constraints to our deep learning system and provide theoretical justification for utilizing transfer learning.
- We define a proxy task to learn the transformation of a 3D nodule to a latent vector based on semantic features defined by medical experts.
- We study semantic information preservation by our system, devise an evaluation technique that considers the lack of consensus between the doctors, and show that our method retrieves highly relevant results.

1.2 Related Work

Most of the previous research uses classic computer vision methods for feature extraction, using a 2D representation of the nodules. This approach fails to capture the full spatial nodule information. A significant challenge in CBIR is the definition of the distance between two entities so that they will be considered semantically similar in addition to being visually similar. Often, the evaluation of the models is hindered by the lack of consensus between human annotators.

A few works in the field include the following: Lam et al.[6] performed CBIR on 2D slices of the 3D nodules using classical image descriptors. Dhara et al.[3] extended this approach with manually defined volumetric features. Pan et al.[13] used spectral clustering to transfer a 3D nodule to hash code used to retrieve similar nodules. Wei et al.[18] proposed a learned distance metric. Finally, Loyman & Greenspan[8] study included LIDC-IDRI rating regression from 2D slices to obtain embeddings using deep learning.

2 Methods

2.1 Data

LIDC-IDRI. The Lung Image Database Consortium and Image Database Resource Initiative (LIDC-IDRI) image collection consists of diagnostic and lung cancer screening thoracic computed tomography (CT) scans with marked-up annotated lesions[2,1]. A panel of four experienced radiologists performed independent segmentation and initial categorization. Lesions categorized as nodules larger than 3mm in diameter were further assessed for nine subjective characteristics: subtlety, internal structure, calcification, sphericity, margin, lobulation, spiculation, radiographic solidity, and malignancy[10]. Each characteristic consists of either a discrete category set or an integer rating on a five-point scale. We use pylidc software [4] to access radiologist annotations.

Analysis of nodule characteristic distribution revealed four characteristics with very low variability between nodules, which we decided to omit from further processing. Adopting the LUNA16 [15] approach we also limited the analysis to nodules accepted by at least three out of four radiologists. This resulted in 1186 nodules, each with three or four sets of segmentation and five-dimensional rating characteristic (subtlety, sphericity, margin, lobulation, and malignancy). We normalize all rating values to $[0, 1]$ range to aid the implementation.

2.2 Methodology

CBIR Using Embeddings. Our approach to CBIR is partially inspired by the natural language processing technique called word2vec[11]. We learn a function $f : V \rightarrow S$ from a high dimensional space of CT voxels V to a much lower dimensional space S , which we call “a semantic space”. A desirable property of S is to capture nodule similarity as perceived by radiology experts, that is, for some distance function $d : S^2 \rightarrow \mathbb{R}$ we expect two vectors $s_1, s_2 \in S$ to be relatively close (have small $d(s_1, s_2)$) if the corresponding nodules would be considered similar by the doctors and vice versa. We call vectors in S “embeddings”. Not necessarily interpretable per se, we would like an embedding to incorporate both characteristic information as defined by radiologists as well as some visual information about the nodule. A traditional approach to learn embeddings is to define a proxy task, such that training a deep learning model to solve this task would produce the embeddings as a byproduct.

Theoretical Architecture Constraints. According to PAC theory (e.g. see [12, ch. 2]) bound of the generalization error over hypothesis space \mathcal{H} and number of training samples N is:

$$R(h) \leq \hat{R}_S(h) + O\left(\sqrt{\frac{\log |\mathcal{H}|}{N}}\right) \quad (1)$$

Our dataset has a very limited number of nodules, while the deep learning network capable of extracting the information from the 3D space of voxels can have

many millions of parameters, that is, $N \ll \log |\mathcal{H}|$. While some researchers question the tightness of such theoretical generalization error bounds, we still wary of the model overfitting in our setting. Therefore, we decide that our proxy task may not be sufficient to train a robust feature extraction.

Feature Extraction. Fortunately, thanks to LUNA16[15] and Kaggle Data Science Bowl (DSB) 2017[5] competitions there are a lot of previous works tackling pulmonary nodule analysis. In this work we apply a transfer learning technique to the winning DSB solution[7] which is based on the U-net architecture[14]. It has initially been trained on a dataset including lots of scans not found in LIDC-IDRI and optimized for different tasks, namely, pulmonary nodule detection and binary whole-scan classification. For our feature extraction, we reuse the pre-trained U-net backbone of the nodule detector and drop the region proposal head comprising of the last two convolutional layers.

Rating Regression. Here we define a proxy task as a radiologist rating regression. We extend the feature extraction network with three fully connected layers with the output being a five-dimensional vector (Figure 1). A target is defined as a mean of radiologist ratings applied to the nodule at hand. We use MSE loss, training only the head while keeping the backbone weights fixed. A ten-dimensional vector from the second-to-last layer is used as an embedding.

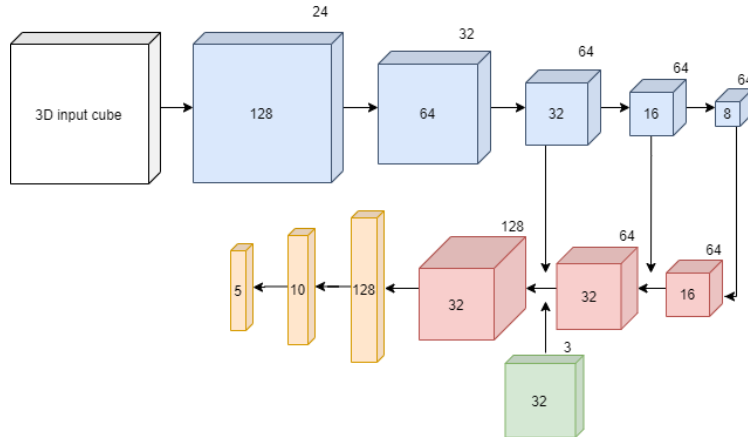


Fig. 1: Regression network for embeddings learning (only feature map is shown). The trainable head comprises of the last three fully connected layers. See [7] for a detailed explanation about the backbone.

3 Results and Discussion

3.1 Semantic Information Preservation

In this section we study whether the embeddings produced by our method preserve semantic meaning, that is, nodules with similar characteristics produce similar embeddings.

t-SNE. We run t-SNE[9] dimensionality reduction over the random sample of the embeddings space (Figure 2a). For simplicity, the coloring here only reflects malignancy: samples with high malignancy (mean rating > 3 out of 5) are colored red and others blue. The separation of red and blue is not ideal because embedding vectors preserve more information than just a malignancy level. However, we observe that the malignant nodules are clustered together, unlike the benign nodules. The more detailed analysis of malignant embeddings reveals that the distance from the center of mass of the red cluster roughly corresponds to the inverse malignancy rating of the nodule (not shown).

Hierarchical Clustering. We also run a hierarchical clustering of a random subset of embeddings using Ward’s minimum variance method[17] (Figure 2b). We analyze the top three splits and observe that the mean malignancy rating of nodules in the leftmost group (green) is much higher than in other groups, that is, the first split happens to cluster malignant vs benign nodules. Similarly, the second split isolates low-margin benign nodules (red) from other benign ones, and finally, the third split differentiates based on subtlety rating (among benign nodules with high margin score).

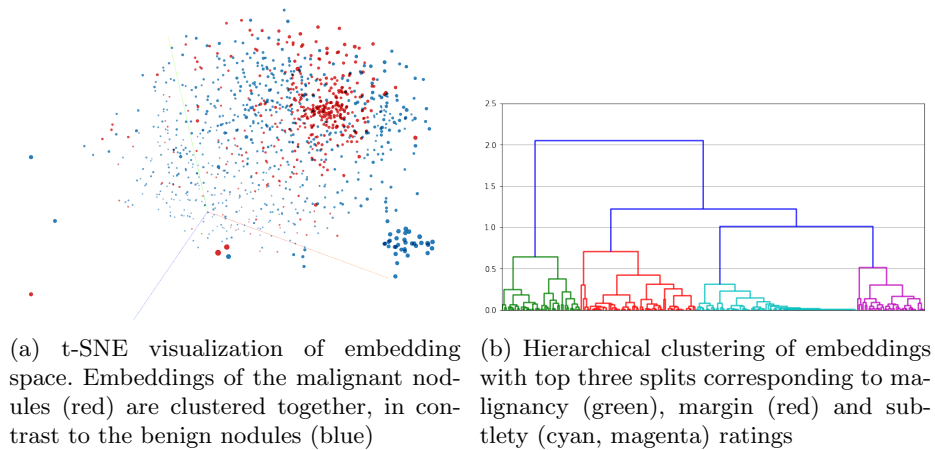


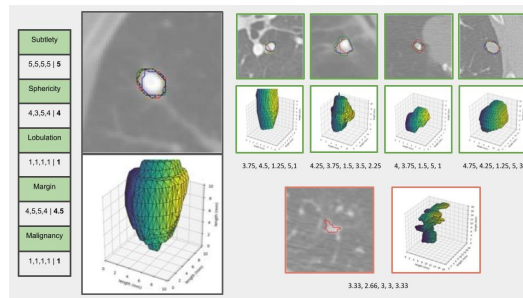
Fig. 2: Semantic information preservation in embedding space

3.2 Usability: Top- k Evaluation

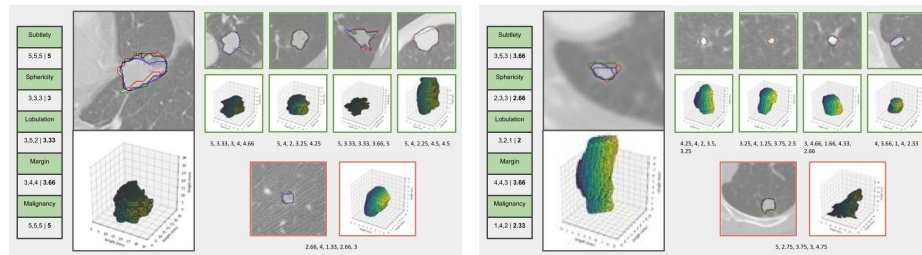
The purpose of our system is to aid a radiologist by presenting top- k cases similar to the query nodule. A radiologist can then inspect each presented case, assessing morphological similarity and reviewing historical diagnosis or even broader clinical records of the patients with presumably similar cases. Aiming for interface simplicity and maximum user productivity we prefer a minimum k which still provides enough information to support a doctor’s decision. We study the semantic space distance between the retrieved samples and a query and decide that beyond $k = 4$ CBIR results provide diminishing returns.

3.3 Qualitative Assessment: Example Output

Figure 3 shows example results of our system. The query nodule is presented on the left side (gray border). Only a single CT slice is shown, with doctors segmentation marks superimposed. A 3D mesh of consensus segmentation is presented below the slice. Query ratings (before normalization) together with the mean are provided on the left. The Top-4 CBIR results are shown on the right (green border) together with their mean ratings. Notice the shape and rating similarity of the CBIR results to that of the query. A non-match nodule is displayed (red border) for comparison. We remind the reader that in contrast to Figure 3 visualization the CBIR query consists of a 3D CT patch only.



(a) Low malignancy query example



(b) High malignancy query example

(c) Uncertain malignancy query example

Fig. 3: CBIR evaluation examples. See subsection 3.3 text for the description.

3.4 Quantitative Assessment

To quantify the CBIR performance we conduct two evaluations: First, we compare the CBIR-based algorithm to medical experts. Then we compare to a recent work in the field [8].

Comparison to Human Experts. We define a nodule rating consensus as a mean vector of ratings assigned to the same nodule by several radiologists. A *dissent score* of the specific radiologist ratings is defined as an RMSE between it and the consensus among other radiologists. Similarly, a *dissent score* of an algorithm is the RMSE between ratings predicted by the algorithm and the consensus of all radiologists (using normalized rating range $[0, 1]$).

We use a rating consensus of k top CBIR results as a naïve algorithm prediction. We also provide, for comparison, a dissent score of a *random algorithm* that predicts one of the existing ratings randomly regardless of the input.

Figure 4 shows a distribution of dissent scores, while Table 1 reports their mean and standard deviation (measured over five-fold cross-validation). We can see that the naïve CBIR-based algorithm for $k = 4$ improves on the doctors’ diagnosis on average as much as the latter improves on a random guess (1.5 times lower mean dissent score). That is, a distance between the query and CBIR results is at least comparable to the ranking uncertainty of the query itself, which is a strong indicator of the embedding space quality.

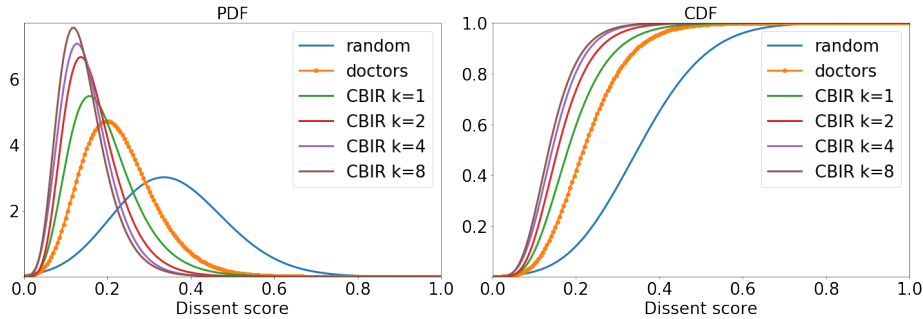


Fig. 4: PDF and CDF of the dissent score of random predictions, doctor ratings, and naïve CBIR-based algorithm with $k \in \{1, 2, 4, 8\}$. For clarity, all graphs show MLE fit of the log-normal distribution. The lower dissent score is better.

Comparison to Recent Results. We extend Table 1 with a comparison to [8]. Following the methodology defined in [8], we compute a prediction RMSE and STD over the dataset for each rating component separately (using rating range $[1, 5]$) and compare to the rating regression results from [8]. We also compute a CBIR malignancy retrieval precision, that is: what portion of the retrieved k

Method	Dissent score		Rating RMSE					Rating STD					Precision
	mean	STD	subtlety	sphericity	lobulation	margin	malignancy	subtlety	sphericity	lobulation	margin	malignancy	
random	0.35	0.13	1.43	1.13	1.27	1.44	1.47	2.81	1.59	2.64	3.08	2.86	
doctors	0.23	0.09	0.72	0.69	0.74	0.73	0.75	0.83	0.64	0.98	0.95	0.85	
CBIR k=1	0.19	0.08	0.89	0.79	0.84	0.94	0.87	0.59	0.48	0.58	0.61	0.56	0.81
CBIR k=2	0.17	0.07	0.76	0.70	0.74	0.81	0.73	0.49	0.41	0.48	0.52	0.47	0.80
CBIR k=4	0.15	0.06	0.70	0.65	0.68	0.74	0.68	0.45	0.38	0.44	0.46	0.44	0.80
CBIR k=8	0.14	0.06	0.66	0.63	0.64	0.70	0.64	0.43	0.37	0.42	0.44	0.41	0.79
CBIR mean													0.79
Loyman et al.			0.93	0.83	0.89	0.94	0.68	0.84	0.47	0.27	0.37	0.84	0.75

Table 1: Quantitative comparison of methods: Random guess, human expert, presented CBIR solution (“CBIR”), and Loyman et al [8]. For the RMSE-based metrics, as defined here and in [8], lower is better. For Retrieval precision, higher is better. The best results are in bold.

results has a correct binary malignancy class (benign vs malignant). Since [8] only presents mean precision for $k \in \{1, 3, 5, 7, 9, 11, 13, 15\}$ we compute it as well for a meaningful comparison (“CBIR mean” in the Table). From the results shown in the Table, we can see that our CBIR-based rating prediction improves over [8] by 0.20 for RMSE and by 0.14 for STD on average. It also compares favorably to human experts. The retrieval precision is improved by 4%.

4 Conclusion

In this work we prototype a CBIR system for pulmonary nodules. We develop a methodology to learn low-dimensional embeddings and present a theoretical justification for the architectural design selected. Our methodology facilitates learning of high-quality embeddings preserving both spatial and semantic information, all this despite very high data dimensionality and sample scarcity. We determine optimal usability settings and perform a qualitative analysis of CBIR results. Finally, we conduct a quantitative study demonstrating state-of-the-art results. While we believe that in reality, the diagnostic process is more complex than a 5-tuple rating can convey, we conclude that the CBIR output is highly relevant to the query, such that the benefit provided by the system to the radiologist end-user is comparable to obtaining a second radiologist’s opinion.

Acknowledgments. Part of the work presented in this paper was done by the first two authors in the course of Y-Data program by Yandex School of Data Analysis. The authors would like to thank Kostya Kilimnik and Shlomo Kashani for the organization and support of the project initiation.

References

1. Armato, S.G., McLennan, G., Bidaut, L., McNitt-Gray, M.F., Meyer, C.R., Reeves, A.P., Zhao, B., Aberle, D.R., Henschke, C.I., Hoffman, E.A., Kazerooni, E.A., MacMahon, H., van Beek, E.J.R., Yankelevitz, D., Biancardi, A.M., Bland, P.H., Brown, M.S., Engelmann, R.M., Laderach, G.E., Max, D., Pais, R.C., Qing, D.P.Y., Roberts, R.Y., Smith, A.R., Starkey, A., Batra, P., Caligiuri, P., Farooqi, A., Gladish, G.W., Jude, C.M., Munden, R.F., Petkovska, I., Quint, L.E., Schwartz, L.H., Sundaram, B., Dodd, L.E., Fenimore, C., Gur, D., Petrick, N., Freymann, J., Kirby, J., Hughes, B., Castele, A.V., Gupte, S., Sallam, M., Heath, M.D., Kuhn, M.H., Dharaiya, E., Burns, R., Fryd, D.S., Salganicoff, M., Anand, V., Shreter, U., Vastagh, S., Croft, B.Y., Clarke, L.P.: The lung image database consortium (LIDC) and image database resource initiative (IDRI): A completed reference database of lung nodules on CT scans. *Medical Physics* **38**(2), 915–931 (Jan 2011). <https://doi.org/10.1118/1.3528204>
2. Armato III, Samuel G., McLennan, G., Bidaut, L., McNitt-Gray, M.F., Meyer, C.R., Reeves, A.P., Zhao, B., Aberle, D.R., Henschke, C.I., Hoffman, E.A., Kazerooni, E.A., MacMahon, H., Van Beek, E.J., Yankelevitz, D., Biancardi, A.M., Bland, P.H., Brown, M.S., Engelmann, R.M., Laderach, G.E., Max, D., Pais, R.C., Qing, D.P., Roberts, R.Y., Smith, A.R., Starkey, A., Batra, P., Caligiuri, P., Farooqi, A., Gladish, G.W., Jude, C.M., Munden, R.F., Petkovska, I., Quint, L.E., Schwartz, L.H., Sundaram, B., Dodd, L.E., Fenimore, C., Gur, D., Petrick, N., Freymann, J., Kirby, J., Hughes, B., Castele, A.V., Gupte, S., Sallam, M., Heath, M.D., Kuhn, M.H., Dharaiya, E., Burns, R., Fryd, D.S., Salganicoff, M., Anand, V., Shreter, U., Vastagh, S., Croft, B.Y., Clarke, L.P.: Data from lidc-idri (2015). <https://doi.org/10.7937/K9/TCIA.2015.LO9QL9SX>, <https://wiki.cancerimagingarchive.net/x/rgAe>
3. Dhara, A.K., Mukhopadhyay, S., Dutta, A., Garg, M., Khandelwal, N.: Content-based image retrieval system for pulmonary nodules: Assisting radiologists in self-learning and diagnosis of lung cancer. *Journal of Digital Imaging* **30**(1), 63–77 (Sep 2016). <https://doi.org/10.1007/s10278-016-9904-y>
4. Hancock, M.C., Magnan, J.F.: Lung nodule malignancy classification using only radiologist-quantified image features as inputs to statistical learning algorithms: probing the lung image database consortium dataset with two statistical learning methods. *Journal of Medical Imaging* **3**(4), 044504 (Dec 2016). <https://doi.org/10.1117/1.jmi.3.4.044504>
5. Kaggle data science bowl 2017 (2017), <https://www.kaggle.com/c/data-science-bowl-2017>, accessed: Jan 2020
6. Lam, M.O., Disney, T., Raicu, D.S., Furst, J., Channin, D.S.: BRISC—an open source pulmonary nodule image retrieval framework. *Journal of Digital Imaging* **20**(S1), 63–71 (Aug 2007). <https://doi.org/10.1007/s10278-007-9059-y>
7. Liao, F., Liang, M., Li, Z., Hu, X., Song, S.: Evaluate the malignancy of pulmonary nodules using the 3-d deep leaky noisy-OR network. *IEEE Transactions on Neural Networks and Learning Systems* **30**(11), 3484–3495 (Nov 2019). <https://doi.org/10.1109/tnnls.2019.2892409>
8. Loyman, M., Greenspan, H.: Lung nodule retrieval using semantic similarity estimates. In: Hahn, H.K., Mori, K. (eds.) *Medical Imaging 2019: Computer-Aided Diagnosis*. SPIE (Mar 2019). <https://doi.org/10.1117/12.2512115>
9. Maaten, L.v.d., Hinton, G.: Visualizing data using t-sne. *Journal of machine learning research* **9**(Nov), 2579–2605 (2008)

10. McNitt-Gray, M.F., Armato, S.G., Meyer, C.R., Reeves, A.P., McLennan, G., Pais, R.C., Freymann, J., Brown, M.S., Engelmann, R.M., Bland, P.H., Laderach, G.E., Piker, C., Guo, J., Towfic, Z., Qing, D.P.Y., Yankelevitz, D.F., Aberle, D.R., van Beek, E.J., MacMahon, H., Kazerooni, E.A., Croft, B.Y., Clarke, L.P.: The lung image database consortium (LIDC) data collection process for nodule detection and annotation. *Academic Radiology* **14**(12), 1464–1474 (Dec 2007). <https://doi.org/10.1016/j.acra.2007.07.021>
11. Mikolov, T., Chen, K., Corrado, G., Dean, J.: *Efficient estimation of word representations in vector space* (2013)
12. Mohri, M., Rostamizadeh, A., Talwalkar, A.: *Foundations of Machine Learning*. The MIT Press, 2nd edn. (dec 2018)
13. Pan, L., Qiang, Y., Yuan, J., Wu, L.: Rapid retrieval of lung nodule CT images based on hashing and pruning methods. *BioMed Research International* **2016**, 1–10 (2016). <https://doi.org/10.1155/2016/3162649>
14. Ronneberger, O., Fischer, P., Brox, T.: U-net: Convolutional networks for biomedical image segmentation. In: *Medical Image Computing and Computer-Assisted Intervention – MICCAI 2015*, pp. 234–241. Springer International Publishing (2015). https://doi.org/10.1007/978-3-319-24574-4_28
15. Setio, A.A.A., Traverso, A., de Bel, T., Berens, M.S., van den Bogaard, C., Cerello, P., Chen, H., Dou, Q., Fantacci, M.E., Geurts, B., van der Gugten, R., Heng, P.A., Jansen, B., de Kaste, M.M., Kotov, V., Lin, J.Y.H., Manders, J.T., Sónora-Mengana, A., García-Naranjo, J.C., Papavasileiou, E., Prokop, M., Saletta, M., Schaefer-Prokop, C.M., Scholten, E.T., Scholten, L., Snoeren, M.M., Torres, E.L., Vandemeulebroucke, J., Walasek, N., Zuidhof, G.C., van Ginneken, B., Jacobs, C.: Validation, comparison, and combination of algorithms for automatic detection of pulmonary nodules in computed tomography images: The LUNA16 challenge. *Medical Image Analysis* **42**, 1–13 (Dec 2017). <https://doi.org/10.1016/j.media.2017.06.015>
16. Siegel, R.L., Miller, K.D., Jemal, A.: Cancer statistics, 2020. *CA: A Cancer Journal for Clinicians* **70**(1), 7–30 (Jan 2020). <https://doi.org/10.3322/caac.21590>
17. Ward, J.H.: Hierarchical grouping to optimize an objective function. *Journal of the American Statistical Association* **58**(301), 236–244 (Mar 1963). <https://doi.org/10.1080/01621459.1963.10500845>
18. Wei, G., Ma, H., Qian, W., Jiang, H., Zhao, X.: Content-based retrieval for lung nodule diagnosis using learned distance metric. In: *2017 39th Annual International Conference of the IEEE Engineering in Medicine and Biology Society (EMBC)*. IEEE (Jul 2017). <https://doi.org/10.1109/embc.2017.8037711>